The Astrophysical Journal Letters, 885:L28 (8pp), 2019 November 10 https://doi.org/10.3847/2041-8213/ab50bd

Propagation of Solar Energetic Particles in the Outer Heliosphere: Interplay between Scattering and Adiabatic Focusing

H.-Q. He[1,2,3] and W. Wan[1,2,3]
[1] Key Laboratory of Earth and Planetary Physics, Institute of Geology and Geophysics, Chinese Academy of Sciences, Beijing 100029, People's Republic of China
hqhe@mail.iggcas.ac.cn
[2] Innovation Academy for Earth Science, Chinese Academy of Sciences, Beijing 100029, People's Republic of China
[3] Beijing National Observatory of Space Environment, Institute of Geology and Geophysics, Chinese Academy of Sciences, Beijing 100029, People's Republic of China
Received 2019 August 26; revised 2019 October 20; accepted 2019 October 23; published 2019 November 6

Abstract

The turbulence and spatial nonuniformity of the guide magnetic field cause two competitive effects, namely, the scattering effect and the adiabatic focusing effect, respectively. In this work, we numerically solve the five-dimensional Fokker–Planck transport equation to investigate the radial evolutions of these important effects undergone by the solar energetic particles (SEPs) propagating through interplanetary space. We analyze the interplay process between the scattering and adiabatic focusing effects in the context of three-dimensional propagation, with special attention to the scenario of the outer heliosphere, in which some peculiar SEP phenomena are found and explained. We also discuss the radial dependence of the SEP peak intensities from the inner through the outer heliosphere, and conclude that it cannot be simply described by a single functional form such as $R^{-\alpha}$ (R is radial distance), which is often used.

Unified Astronomy Thesaurus concepts: Interplanetary turbulence (830); Interplanetary medium (825); Solar particle emission (1517); Solar energetic particles (1491); Solar magnetic fields (1503); Heliosphere (711)

1. Introduction

Solar energetic particles (SEPs) are produced near the Sun during solar eruptive events and will transport in the interplanetary space filled with turbulent magnetic fields. The SEP events observed in the heliosphere provide fundamental information regarding particle acceleration and transport mechanisms, which are enigmatic problems of long-standing importance in space physics, plasma physics, and astrophysics. Therefore, the SEPs can serve as convenient messengers for us to achieve a better understanding of the fundamental behaviors of energetic particles in extreme astrophysical environments including dynamical plasma media and waves and turbulent magnetic fields. In the upcoming era of *Parker Solar Probe* and *Solar Orbiter*, it is expected to make significant advances in understanding the physical mechanisms of particle origin, acceleration, and transport.

The charged energetic particles in magnetic turbulence experience scattering and diffusion processes both parallel and perpendicular to the large-scale guide magnetic field. Parallel diffusion of charged particles along the mean magnetic field has been extensively investigated (e.g., Dröge 2000; Shalchi & Schlickeiser 2005; Shalchi et al. 2006; He & Wan 2012a). Recently, perpendicular diffusion of charged particles across the guide magnetic field has also been intensely studied (e.g., Zhang et al. 2009; Shalchi 2010, 2019; He et al. 2011; Dröge et al. 2014; He 2015). The parallel mean free path $\lambda_{\parallel,0}$ of charged particles in a uniform mean magnetic field can be written as (Jokipii 1966; Hasselmann & Wibberenz 1968; Earl 1974)

$$\lambda_{\parallel,0}=\frac{3v}{8}\int_{-1}^{+1}\frac{(1-\mu^2)^2}{D_{\mu\mu}}d\mu, \tag{1}$$

where $D_{\mu\mu}$ is the pitch-angle diffusion coefficient. However, most of the astrophysical magnetic fields including the interplanetary magnetic fields are often nonuniform. This spatially varying mean magnetic field gives rise to the adiabatic focusing effect of charged energetic particles (Roelof 1969; Earl 1976; Bieber & Burger 1990; Ruffolo 1995; Bieber et al. 2002; Schlickeiser & Shalchi 2008). The presence of the adiabatic focusing effect causes coherent spatial particle streaming along the large-scale guide magnetic field in magnetostatic turbulence. In the scenario of the inner heliosphere, the adiabatic focusing effect is very important and must be taken into account when we analyze the diffusion and transport processes of SEPs in the interplanetary space (He & Wan 2012a). In general, the adiabatic focusing length $L(z)$ can be defined via

$$\frac{1}{L(z)}=-\frac{\partial \ln B(z)}{\partial z}=-\frac{1}{B(z)}\frac{\partial B(z)}{\partial z}, \tag{2}$$

where $B(z)$ is the mean magnetic field with direction z. As we can see, the focusing length $L(z)$ is positive in a diverging guide field and is negative in a converging guide field.

In previous studies, most authors theoretically investigated the effects of magnetic adiabatic focusing on the parallel diffusion coefficients of charged particles (Beeck & Wibberenz 1986; Bieber & Burger 1990; Ruffolo 1995; Kota 2000; Schlickeiser & Shalchi 2008; Litvinenko 2012; Shalchi & Danos 2013; He & Schlickeiser 2014). They usually focused on calculating the modifications of spatial diffusion coefficients of charged particles transporting in nonuniform guide magnetic

fields. During the derivations, a number of useful and universal approximation and perturbation methods have been presented in the literature. However, it is quite scarce to see the investigations within the community that directly analyze the effects of adiabatic focusing on the transport and distribution of SEPs in the inner and the outer heliosphere by presenting the time-intensity profiles of radial evolutions of SEPs, especially in the physical scenario of three-dimensional propagation including perpendicular diffusion. Undoubtedly, such investigation tasks are very important for us to achieve a clear and explicit understanding of the effects of adiabatic focusing on the SEP diffusion, transport, and distribution. In addition, performing such tasks can bring us a detailed illustration of the interplay process between the adiabatic focusing effect and the particle scattering effect. To this aim, it is necessary to numerically simulate the three-dimensional transport processes of SEPs in the inner and the outer heliosphere, since the multidimensional focused transport equation is very difficult to solve analytically.

In this work, we numerically solve the five-dimensional Fokker–Planck transport equation that incorporates all of the essential transport mechanisms including perpendicular diffusion. We analyze the simulation results and investigate the radial evolutions of SEP time-flux profiles from the inner through the outer heliosphere. The effects of adiabatic focusing and SEP scattering and the interplay process between them in the interplanetary magnetic fields will be discussed. Some peculiar SEP phenomena including SEP "floods" (previously "reservoirs") found in the inner and the outer heliosphere will also be analyzed and discussed. This Letter is structured as follows. In Section 2, we present the numerical model used in this work, i.e., the five-dimensional Fokker–Planck focused transport equation, and the relevant simulation method for numerically solving the equation. In Section 3, we present the simulation results and discuss the physical mechanisms, with special attention to the effects of adiabatic focusing and particle scattering. We also present multi-spacecraft observations for comparison with simulations. In Section 4, a summary of our results will be provided.

2. Numerical Model and Method

The five-dimensional time-dependent Fokker–Planck transport equation for the gyrophase-averaged SEP distribution function $f(\boldsymbol{x}, \mu, p, t)$, which incorporates the effects of adiabatic focusing and particle scattering in pitch-angle cosine μ, can be written as (e.g., Schlickeiser 2002; Zhang et al. 2009; He et al. 2011, 2017; Dröge et al. 2014, 2016; He 2015)

$$\frac{\partial f}{\partial t} + \mu v\frac{\partial f}{\partial z} + \boldsymbol{V}^{\rm sw}\cdot\nabla f + \frac{dp}{dt}\frac{\partial f}{\partial p} + \frac{d\mu}{dt}\frac{\partial f}{\partial \mu} - \frac{\partial}{\partial \mu}\left(D_{\mu\mu}\frac{\partial f}{\partial \mu}\right) - \frac{\partial}{\partial x}\left(\kappa_{xx}\frac{\partial f}{\partial x}\right) - \frac{\partial}{\partial y}\left(\kappa_{yy}\frac{\partial f}{\partial y}\right) = Q(\boldsymbol{x}, p, t). \quad (3)$$

In the above Fokker–Planck transport equation, $\boldsymbol{x}$ denotes the spatial position of particles, z denotes the spatial coordinate along the guide magnetic field line $B(z)$, p is particle's momentum, t is time, v is particle's velocity, $\boldsymbol{V}^{\rm sw}$ is solar wind speed, κ_{xx} and κ_{yy} denote perpendicular diffusion coefficients, and $Q(\boldsymbol{x}, p, t)$ denotes particle source term. The term dp/dt, describing the adiabatic cooling effect, can be written as

$$\frac{dp}{dt} = -p\left[\frac{1-\mu^2}{2}\left(\frac{\partial V_x^{\rm sw}}{\partial x} + \frac{\partial V_y^{\rm sw}}{\partial y}\right) + \mu^2\frac{\partial V_z^{\rm sw}}{\partial z}\right]. \quad (4)$$

The term $d\mu/dt$, representing the effect of magnetic adiabatic focusing and the divergence of solar wind flows, can be written as

$$\frac{d\mu}{dt} = \frac{1-\mu^2}{2}\left[-\frac{v}{B}\frac{\partial B}{\partial z} + \mu\left(\frac{\partial V_x^{\rm sw}}{\partial x} + \frac{\partial V_y^{\rm sw}}{\partial y} - 2\frac{\partial V_z^{\rm sw}}{\partial z}\right)\right] = \frac{1-\mu^2}{2}\left[\frac{v}{L} + \mu\left(\frac{\partial V_x^{\rm sw}}{\partial x} + \frac{\partial V_y^{\rm sw}}{\partial y} - 2\frac{\partial V_z^{\rm sw}}{\partial z}\right)\right], \quad (5)$$

where B denotes the guide interplanetary magnetic field, and L denotes the magnetic focusing length.

Accordingly, the radial mean free path λ_r can be expressed as

$$\lambda_r = \lambda_\parallel \cos^2\psi. \quad (6)$$

Here, ψ denotes the angle between the local magnetic field direction and the radial direction. We utilize a pitch-angle diffusion coefficient with the following form (e.g., Beeck & Wibberenz 1986; Zhang et al. 2009; He et al. 2011)

$$D_{\mu\mu}^r = D_{\mu\mu}/\cos^2\psi = D_0 v R_d^{-1/3}(|\mu|^{q-1} + h)(1-\mu^2), \quad (7)$$

where D_0 denotes the magnetic turbulence strength, R_d denotes the particle rigidity, h is a parameter set to describe the particle scattering ability through 90° pitch-angle, and q is a parameter relevant to the power spectrum of the magnetic turbulence in inertial range, which is set to be $5/3$ in this work. Recently, a more accurate expression for the pitch-angle scattering coefficient was derived systematically from nonlinear diffusion theory that also provides a nonvanishing scattering coefficient at $\mu = 0$ (Shalchi et al. 2009). In addition, note that the focusing effect can alter the pitch-angle scattering effects itself (Tautz et al. 2014).

We employ the so-called time-backward Markov stochastic process approach to numerically solve the five-dimensional Fokker–Planck transport Equation (3). Through this approach, the Fokker–Planck Equation (3) can be readily transformed into five time-backward stochastic differential equations (SDEs) as in the following:

$$\begin{aligned} dX &= \sqrt{2\kappa_{xx}}\,dW_x(s) - V_x^{\rm sw}ds \\ dY &= \sqrt{2\kappa_{yy}}\,dW_y(s) - V_y^{\rm sw}ds \\ dZ &= -(\mu V + V_z^{\rm sw})ds \\ d\mu &= \sqrt{2D_{\mu\mu}}\,dW_\mu(s) - \frac{1-\mu^2}{2}\left[\frac{V}{L} + \mu\left(\frac{\partial V_x^{\rm sw}}{\partial x} + \frac{\partial V_y^{\rm sw}}{\partial y} - 2\frac{\partial V_z^{\rm sw}}{\partial z}\right)\right]ds + \left(\frac{\partial D_{\mu\mu}}{\partial \mu} + \frac{2D_{\mu\mu}}{M+\mu}\right)ds \\ dP &= P\left[\frac{1-\mu^2}{2}\left(\frac{\partial V_x^{\rm sw}}{\partial x} + \frac{\partial V_y^{\rm sw}}{\partial y}\right) + \mu^2\frac{\partial V_z^{\rm sw}}{\partial z}\right]ds, \end{aligned} \quad (8)$$

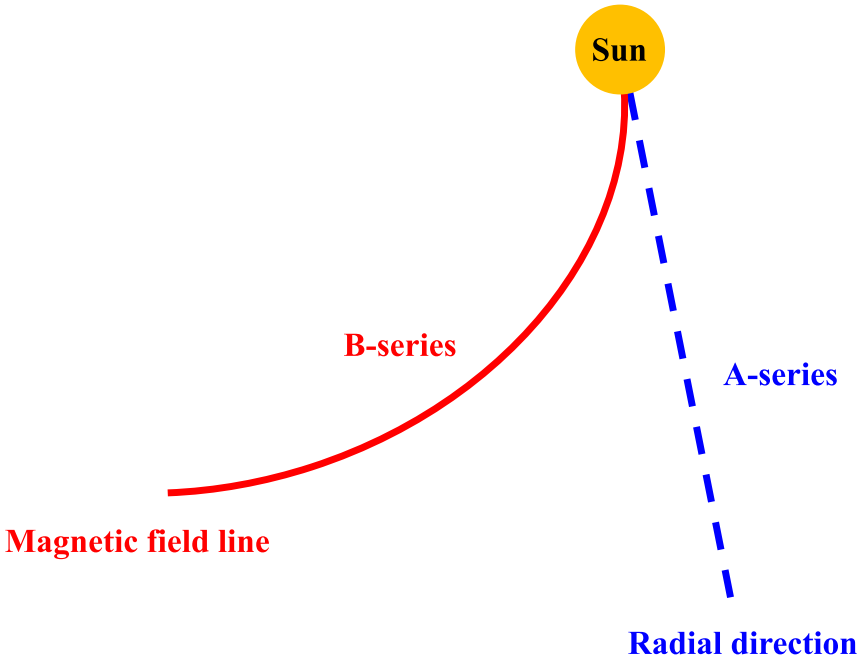

Figure 1. Illustrative sketch to show the alignment scenarios of the spacecraft fleet in the heliosphere. The blue dashed line denotes the radial direction along which the A-series spacecraft are aligned with different radial distances. The red solid curve indicates the interplanetary magnetic field line along which the B-series spacecraft are aligned with different radial distances. The heliocentric radial distances of the spacecraft fleet in each alignment are in sequence: 0.25, 0.4, 0.6, 0.8, 1.0, 1.5, 2.0, 2.5, 3.0, 3.5, 4.0, 4.5, and 5.0 au. Both the spacecraft fleet and the SEP sources are located at 90° colatitude.

where (X, Y, Z) denotes the particle pseudo-position, V denotes the particle pseudo-speed, P denotes the particle pseudo-momentum, and $W_x(t)$, $W_y(t)$, and $W_\mu(t)$ denote the Wiener processes. The quantity of the gyrophase-averaged particle distribution function $f(\boldsymbol{x}, \mu, p, t)$ can be numerically obtained from the five SDEs (8). In the numerical simulations, we trace a number of particles back to the initial time of the physical system. In the statistical analyses, we only take into account those "effective" particles that arrive at the source region at the initial time.

The particle source term $Q(\boldsymbol{x}, p, t)$ in the Fokker–Planck transport Equation (3), which serves as an inner injection boundary of particles in the simulations, is assumed to be as (Reid 1964)

$$Q(R \leqslant 0.05\ \mathrm{au}, \theta, \phi, E_k, t) = \frac{C}{t}\frac{E_k^{-\gamma}}{p^2}\exp\left(-\frac{\tau_c}{t} - \frac{t}{\tau_L}\right)\xi(\theta, \phi), \quad (9)$$

where γ denotes the spectral index of source region particles that is chosen to be 3, τ_c and τ_L denote the time quantities that determine the particle injection profile in source regions, and $\xi(\theta, \phi)$ is a function controlling the spatial variation (longitude and latitude) of particle injection strength in source regions. We note that the SEP injection model shown in Equation (9) can be used to describe either the SEP release from solar flares or the SEP injections from shocks driven by coronal mass ejections in the corona. This SEP source model is particularly suitable for describing the short-lived injections of high-energy particles released near the Sun. In this work, we concentrate on the SEP time-intensity profiles in the prompt component of SEP events.

In addition, we set an outer boundary at radial distance $R = 50$ au for absorbing the particles when they hit the boundary. For the interplanetary conditions, we typically use a constant solar wind speed of $V^{\mathrm{sw}} = 400\ \mathrm{km\ s^{-1}}$, and a spiral-type interplanetary magnetic field with strength $B = 5$ nT at 1 au. For each SEP case, we simulate 3×10^7 test particles on a supercomputer cluster. During the data analyses of the simulation results, we adopt an arbitrary unit for presenting the time-flux profiles of particles instead of using the usual $\mathrm{cm^{-2}\ s^{-1}\ sr^{-1}\ MeV^{-1}}$, because of the consideration of convenience in plotting figures.

3. Numerical Results and Discussion

We first present an illustrative sketch, i.e., Figure 1, to show the physical scenarios discussed in this Letter. The blue dashed line in Figure 1 denotes the radial direction along which the A-series spacecraft are aligned with different radial distances. The red solid curve indicates the interplanetary magnetic field line along which the B-series spacecraft are aligned with different radial distances. Both the radial direction line and the magnetic field line originate from the same SEP source near the Sun. The heliocentric radial distances of the spacecraft fleet in each alignment scenario (A-series and B-series) are in sequence: 0.25, 0.4, 0.6, 0.8, 1.0, 1.5, 2.0, 2.5, 3.0, 3.5, 4.0, 4.5, and 5.0 au. In addition, both the spacecraft fleet and the SEP sources are located at 90° colatitude. In the simulations, the SEP sources are set to be with limited coverages, i.e., 45° or 70° in longitude and latitude.

Figure 2 presents the observations (top panel) and simulation results (middle and bottom panels) of the radial evolutions of SEP time-flux profiles from the inner through the outer heliosphere. In the top panel, the red solid circles denote the time-flux profiles of 0.9–1.2 MeV protons (30 minute average) observed by *IMP*-8 spacecraft at 1.0 au, and the blue solid circles denote the time-flux profiles of 0.88–1.15 MeV protons (10 minute average) observed by *Ulysses* spacecraft at 2.5 au. The measurements of particle fluxes on both spacecraft were

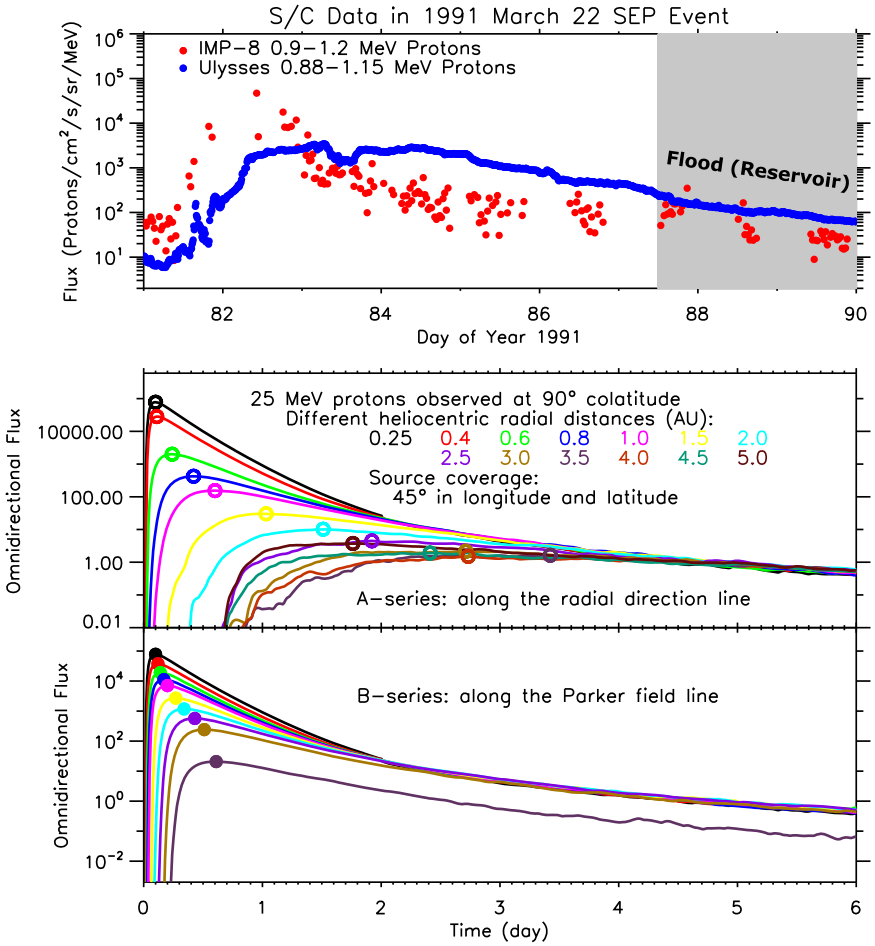

Figure 2. Observations (top) and simulation results (middle and bottom) of the radial evolutions of SEP time-flux profiles from the inner through the outer heliosphere. Top panel: 0.9–1.2 MeV protons (red circles, 30 minute average) observed by *IMP*-8 at 1.0 au and 0.88–1.15 MeV protons (blue circles, 10 minute average) observed by *Ulysses* at 2.5 au during the 1991 March 22 (day of year 81) SEP event. For the simulations, the middle panel denotes the SEP scenario along the radial direction, and the bottom panel denotes the scenario along the interplanetary magnetic field line originating from the SEP source. The particles are 25 MeV protons, and the SEP source is 45° wide in latitude and longitude. The different colors of the time-flux profiles indicate the simulations at different radial distances: 0.25, 0.4, 0.6, 0.8, 1.0, 1.5, 2.0, 2.5, 3.0, 3.5, 4.0, 4.5, and 5.0 au. The open and solid circles on the time-flux profiles in the middle (A-series) and bottom (B-series) panels, respectively, denote the peak fluxes of the corresponding SEP cases.

made during the 1991 March 22 (day of year 81) SEP event. Note that there are data gaps in the time-flux profiles. As we can see, the phase of the rise and the peak of the particle fluxes is quite different at *IMP*-8 and *Ulysses*, but during the late phase (indicated by the gray shaded area), the fluxes at 1.0 au and at 2.5 au are very nearly equal and evolve similarly in time with almost the same decay rates. This particle behavior is the so-called SEP "flood" (previously "reservoir") phenomenon (McKibben 1972; Roelof et al. 1992; He & Wan 2017). Note that the SEP "floods" (previously "reservoirs") are observed in both low- and high-energy particle data, and also in both proton data and electron and heavy-ion data. This SEP phenomenon is detected by spacecraft at different heliolongitudes, heliolatitudes, and radial distances. The middle and bottom panels of Figure 2 present the simulation results of two different SEP scenarios. In the middle panel, the time-flux profiles are observed along the radial direction. In the bottom panel, the time-flux profiles are detected along the Parker-type interplanetary magnetic field line. In the simulation scenarios of middle and bottom panels, the coverage of particle source is set to be 45° both in longitude and latitude. In these two panels, the different colors of the time-flux profiles indicate the simulation results obtained at different radial distances: 0.25, 0.4, 0.6, 0.8, 1.0, 1.5, 2.0, 2.5, 3.0, 3.5, 4.0, 4.5, and 5.0 au. For both scenarios of spacecraft alignment ("A-series" and "B-series"), the SEP diffusion coefficients are set as follows: the radial mean free path $\lambda_r = 0.25$ au (corresponding to the parallel mean free path $\lambda_\parallel = 0.5$ au at 1 au), and the perpendicular mean free paths $\lambda_x = \lambda_y = 0.006$ au. Note that the values of the parallel and perpendicular mean free paths are based on the recent results of observations and theories regarding the parallel and perpendicular diffusion coefficients of energetic charged particles in the interplanetary space (e.g., Bieber et al. 1994, 2004; Dröge 2000; Matthaeus et al. 2003; He & Wan 2012a, 2012b). In the middle panel, we can see that the SEP intensities monotonically decrease with increasing radial distances in the inner heliosphere and as far as ~4.0 au, beyond where the particle intensities counterintuitively and gradually increase with the increasing radial distances up to at least 5.0 au. The reason is that at relatively large radial distances, e.g., at $\gtrsim$3.2 au computed assuming a solar wind speed of 400 km s^{-1}, the larger the radial distance of the observer is, the closer the magnetic footpoint of the observer is to the SEP source, and consequently in the sense of longitudinal distance, the higher the particle flux observed will be. As one can see, during the late phases, the particle intensities of the SEP events present nearly

equal values and evolve similarly in time with almost the same decay rates. This evolution feature of SEP events is the so-called SEP "flood" (previously "reservoir") phenomenon as described in the top panel. Therefore, we successfully reproduce this famous SEP phenomenon by simulating the SEP three-dimensional transport process from the inner through the outer heliosphere. In the bottom panel of Figure 2, the particle intensities gradually decrease with increasing radial distances in the inner heliosphere and up to ~3.0 au. However, at $\gtrsim$3.5 au, the SEP intensity abruptly decreases to a quite low value. Furthermore, the particles almost "disappear" at radial distances $\gtrsim$4.0 au. The reason is that at large radial distances from the Sun, the adiabatic focusing effect is significantly reduced (He & Wan 2012a), and as a result, the particles considerably deviate from the primary magnetic field lines, which they previously followed during the early stage. As one can see in the bottom panel of Figure 2, the so-called SEP "flood" (previously "reservoir") phenomenon (McKibben 1972; Roelof et al. 1992; He & Wan 2017) is successfully reproduced in our three-dimensional transport modeling of SEP propagation from the inner to the outer heliosphere. We note that the open and solid circles on the time-flux profiles in the middle (A-series) and bottom (B-series) panels of Figure 2, respectively, denote the peak fluxes of the corresponding SEP cases. These peak fluxes and their radial evolutions will be discussed later.

Figure 3 shows the numerical simulation results of the radial variations of the time-flux profiles of 32 MeV solar protons transporting from the inner to the outer heliosphere. According to the recent results of observations and theories (e.g., Dröge 2000; Matthaeus et al. 2003; Bieber et al. 2004; He & Wan 2012a, 2012b), the diffusion coefficients of the energetic particles are typically set as follows: the radial mean free path $\lambda_r = 0.28$ au (corresponding to the parallel mean free path $\lambda_{\parallel} = 0.56$ au at 1 au), and the perpendicular mean free paths $\lambda_x = \lambda_y = 0.007$ au. Other physical conditions and modeling parameters are set the same as the simulations in the middle and bottom panels of Figure 2. In the upper panel of Figure 3, one can see that the SEP fluxes monotonically decline with increasing radial distances in the inner heliosphere and up to ~4.0 au. However, afterward the SEP intensities gradually increase with the increasing radial distances as far as at least 5.0 au. This peculiar SEP phenomenon results from the fact that at relatively large radial distances, e.g., at $\gtrsim$3.2 au in this work, the larger the observer's radial distance is, the closer the observer's magnetic footpoint is to the SEP source in longitude, and as a result, the higher the SEP intensity measured will be. In the lower panel of Figure 3, the SEP fluxes gradually decline with increasing radial distances in the inner heliosphere and up to ~3.0 au. Nevertheless, the SEP flux dramatically declines to a very low magnitude at $\gtrsim$3.5 au. Further, the SEP intensities almost "vanish away" at radial distances $\gtrsim$4.0 au. The reason is that at large radial distances, the effect of adiabatic focusing is largely reduced (He & Wan 2012a), and consequently the SEPs significantly deviate from the primary magnetic field lines originating from the limited source region. Note that in both panels, the SEP "flood" (previously "reservoir") phenomenon is reproduced. The open and solid circles on the time-flux profiles in the upper and lower panels of Figure 3, respectively, indicate the peak intensities of the corresponding SEP cases.

Figure 4 presents the radial evolutions of the peak intensities of 25 MeV (solid lines) and 32 MeV (dashed lines) proton events, which are extracted from the simulation results in Figures 2 and 3, respectively. The solid and open circles denote the peak intensities of the SEP events observed along the magnetic field line (B-series) and along the radial direction (A-series), respectively. The coverage of the source region of all the SEP events is 45° in longitude and latitude. We can clearly see that the SEP peak intensities generally decrease with increasing radial distances. However, the evolution process is complicated and cannot be described by a single simple functional form such as power-law function $R^{-\alpha}$ (R is radial distance). Specifically, for both particle energies 25 and 32 MeV, the peak particle intensities of the B-series SEP cases gradually decrease with increasing radial distances up to ~3.0 au, beyond where the peak intensities abruptly decrease to a very low value, due to the significant reduction of the adiabatic focusing effect at large radial distances (He & Wan 2012a). For both 25 and 32 MeV protons, the peak intensities of the A-series SEP cases generally decrease with increasing radial distances up to ~4.0 au, beyond where the peak SEP fluxes counterintuitively increase with the increasing radial distances, due to the decreasing longitudinal separations between the SEP source and the magnetic footpoints of observers at $\gtrsim$3.2 au. As we know, the farther the magnetic footpoint of the observer is away from the SEP source in longitude, the smaller the particle intensity (including peak intensity) observed will be (He et al. 2011). In general, the radial evolution process of SEP intensities is the manifestation of the competitive combination of various fundamental mechanisms such as particle scattering and adiabatic focusing. The competition between scattering and adiabatic focusing is especially meaningful in the outer heliosphere, where the interplay between these two effects may lead to the counter-streaming particle beams (He 2015).

We also numerically simulate the SEP events with the source coverage of 70° in longitude and latitude. Figure 5 presents the simulation results of the radial evolutions of such SEP cases. We note that except for the source coverage, all of the other parameters of the simulations displayed in Figure 5 are the same as the parameters used in Figure 4. As we can see, basically, the evolution trend and evolution property of the SEP events presented in Figure 5 are similar to those in Figure 4. In the beginning, the SEP peak intensities decrease with increasing radial distances. However, the evolution process is complicated and cannot be depicted by a single function such as $R^{-\alpha}$, especially at large radial distances. For both energy channels, the peak intensities in the B-series SEP cases decrease in a gradual manner with increasing radial distances up to ~3.0 au, beyond where the peak intensities suddenly decline to quite a low value, due to the largely reduced focusing effect in the outer heliosphere. In the A-series SEP cases, the peak intensities decrease with increasing radial distances up to ~4.0 au, beyond where the peak fluxes increase with the increasing radial distances, due to the decreasing longitudinal separations between the particle source and the magnetic footpoints of spacecraft at $\gtrsim$3.2 au. Because the decreasing longitudinal distances between SEP source and spacecraft footpoints indicate increasing particle intensities observed by these spacecraft (He et al. 2011). Therefore, the radial evolution of SEP events is an interplay process between particle scattering and adiabatic focusing.

In 1987 March, a workshop on the interplanetary particle environment was held at the Jet Propulsion Laboratory in

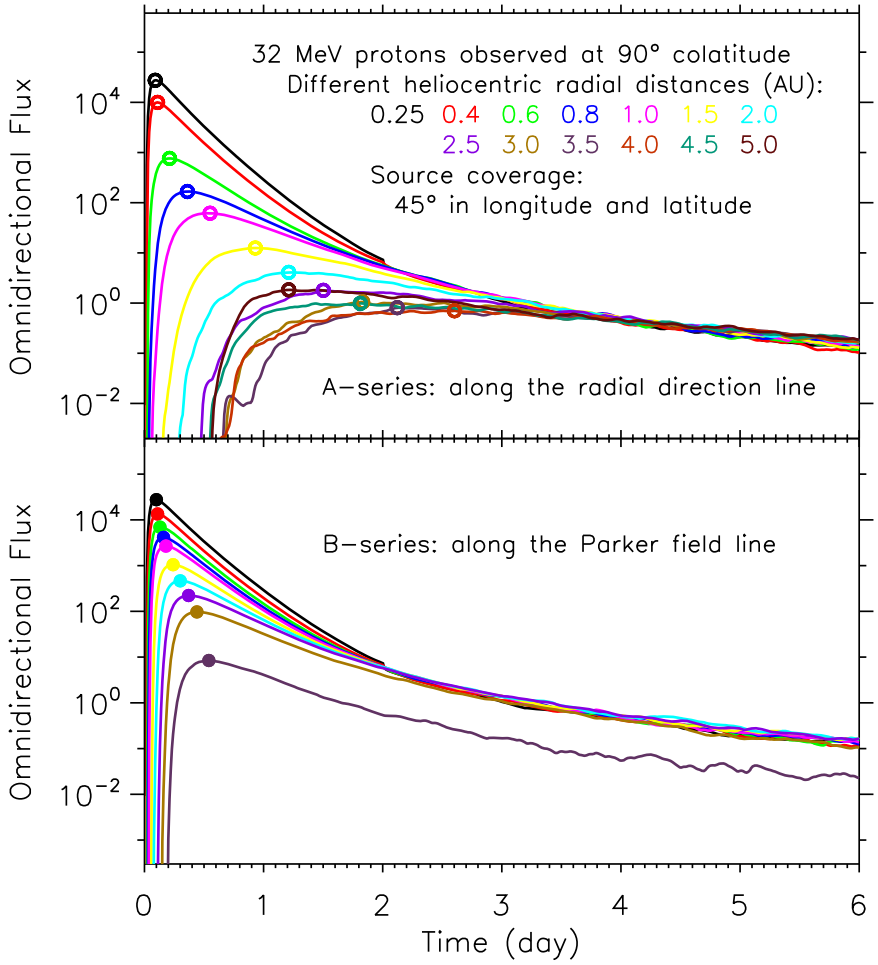

Figure 3. Same as the simulations (middle and bottom panels) in Figure 2, except for 32 MeV protons.

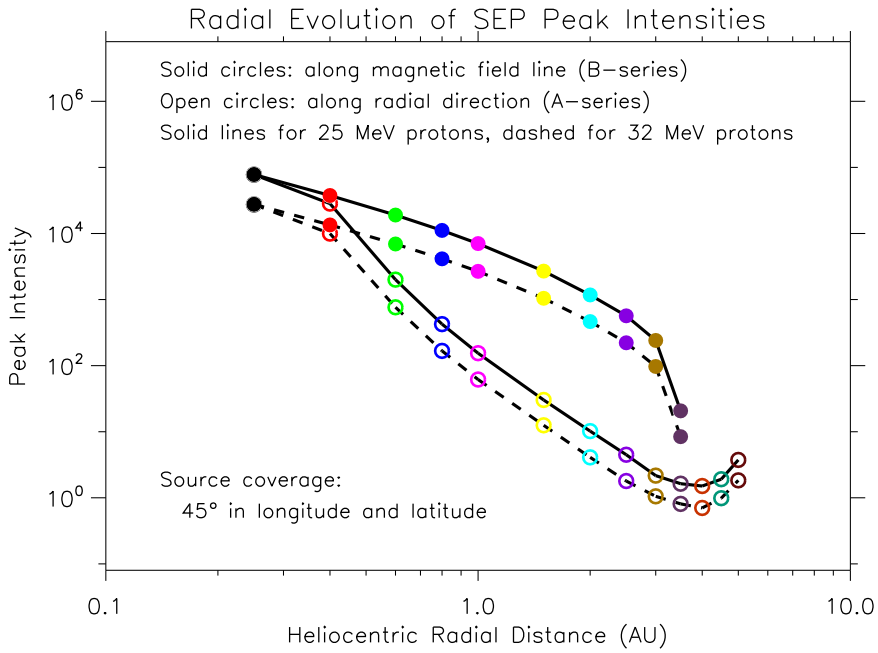

Figure 4. Radial evolutions of the peak fluxes of 25 MeV (solid lines) and 32 MeV (dashed lines) proton events, extracted from the simulation results in Figures 2 and 3, respectively. The solid and open circles denote the SEP peak fluxes observed along the magnetic field line (B-series) and along the radial direction (A-series), respectively. The SEP source is 45° wide in latitude and longitude. The radial evolution of SEP events is a complex interplay process with competition between the effects of particle scattering and adiabatic focusing.

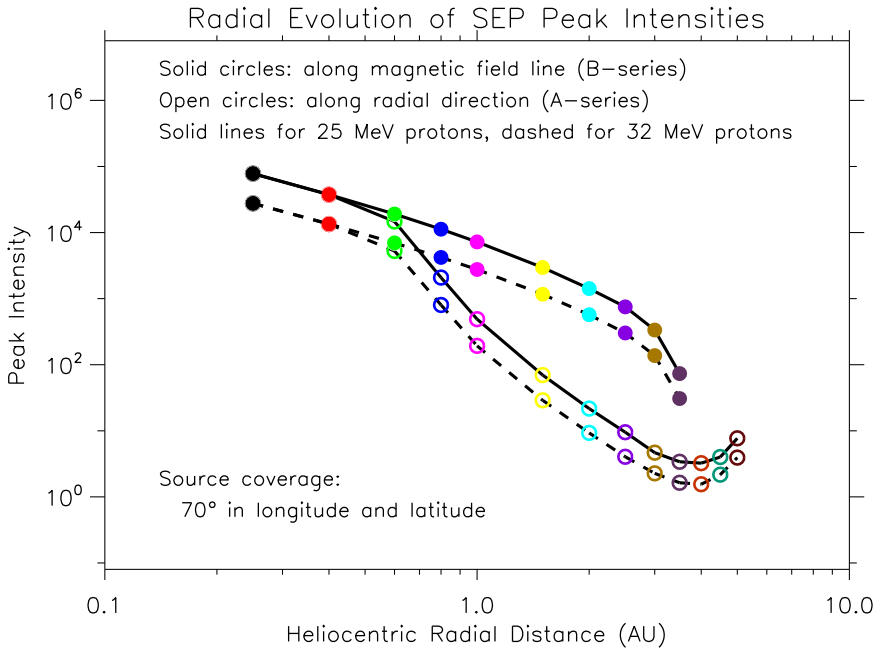

Figure 5. Same as Figure 4, except for the SEP source of 70° width in latitude and longitude.

Pasadena, California. In this workshop, recommendations for radial extrapolation of peak particle fluxes detected at 1 au to other radial distances were adopted by the working group consensus and read as follows (Feynman & Gabriel 1988):

1. To infer proton intensities at radial distances $R > 1$ au from the intensity measurements at 1 au, use a function $R^{-3.3}$ with variations from R^{-4} to R^{-3}.
2. To infer proton intensities at radial distances $R < 1$ au from the intensity measurements at 1 au, use a function R^{-3} with variations from R^{-3} to R^{-2}.

From our simulation results, we can see that the radial evolution of SEP events is a quite complicated process that incorporates several fundamental mechanisms such as particle scattering and adiabatic focusing. The evolution process cannot be simply described by a functional form of $R^{-\alpha}$, especially in the outer heliosphere, where the competitive interplay between the effects of scattering and adiabatic focusing is quite considerable. Therefore, the consensus recommendations for radial extrapolation of SEP intensities empirically adopted during the 1987 workshop are oversimple.

4. Summary and Conclusion

In this work, we investigate the three-dimensional propagation and radial evolution of SEPs from the inner through the outer heliosphere by numerically solving the five-dimensional Fokker–Planck transport equation incorporating the perpendicular diffusion mechanism. We analyze the effects of adiabatic focusing and scattering on the SEP intensities. The interplay process between these effects is discussed in detail by investigating the radial evolution of SEP time-intensity profiles. Some peculiar and interesting phenomena of SEP transport in the three-dimensional interplanetary magnetic field are found for the first time, to our knowledge. For instance, at large radial distances from the Sun, the particle intensities in the B-series SEP cases abruptly decline to a quite low value, and on the contrary, the particle intensities in the A-series SEP cases increase with the increasing radial distances. We discuss the physical mechanisms responsible for the formation of these peculiar SEP phenomena and conclude that these SEP evolution behaviors result from the interplay process between particle scattering and adiabatic focusing. We analyze the radial dependence of SEP peak intensities from the inner through the outer heliosphere and point out that it cannot be described merely by a single functional form $R^{-\alpha}$, especially at large radial distances. We also numerically reproduce the famous SEP "flood" (previously "reservoir") phenomenon from the inner through the outer heliosphere. In addition, our findings can also be used to predict the observations made by future missions in the interplanetary space.

This work was supported in part by the National Natural Science Foundation of China under grants 41621063, 41874207, 41474154, and 41204130, and the Chinese Academy of Sciences under grant KZZD-EW-01-2. H.-Q.H. gratefully acknowledges the partial support of the Youth Innovation Promotion Association of the Chinese Academy of Sciences (No. 2017091). We benefited from the energetic particle data of *IMP*-8 and *Ulysses* provided by NASA/Space Physics Data Facility (SPDF)/CDAWeb.

References

Beeck, J., & Wibberenz, G. 1986, ApJ, 311, 437
Bieber, J. W., & Burger, R. A. 1990, ApJ, 348, 597
Bieber, J. W., Dröge, W., Evenson, P. A., et al. 2002, ApJ, 567, 622
Bieber, J. W., Matthaeus, W. H., Shalchi, A., & Qin, G. 2004, GeoRL, 31, L10805
Bieber, J. W., Matthaeus, W. H., Smith, C. W., et al. 1994, ApJ, 420, 294
Dröge, W. 2000, SSRv, 93, 121
Dröge, W., Kartavykh, Y. Y., Dresing, N., Heber, B., & Klassen, A. 2014, JGRA, 119, 6074
Dröge, W., Kartavykh, Y. Y., Dresing, N., & Klassen, A. 2016, ApJ, 826, 134
Earl, J. A. 1974, ApJ, 193, 231
Earl, J. A. 1976, ApJ, 205, 900
Feynman, J., & Gabriel, S. 1988, Interplanetary Particle Environment, JPL Publication 88-28 (Pasadena, CA: Jet Propulsion Laboratory)
Hasselmann, K., & Wibberenz, G. 1968, ZGeo, 34, 353
He, H.-Q. 2015, ApJ, 814, 157
He, H.-Q., Qin, G., & Zhang, M. 2011, ApJ, 734, 74

He, H.-Q., & Schlickeiser, R. 2014, ApJ, 792, 85
He, H.-Q., & Wan, W. 2012a, ApJ, 747, 38
He, H.-Q., & Wan, W. 2012b, ApJS, 203, 19
He, H.-Q., & Wan, W. 2017, MNRAS, 464, 85
He, H.-Q., Zhou, G., & Wan, W. 2017, ApJ, 842, 71
Jokipii, J. R. 1966, ApJ, 146, 480
Kota, J. 2000, JGR, 105, 2403
Litvinenko, Y. E. 2012, ApJ, 752, 16
Matthaeus, W. H., Qin, G., Bieber, J. W., & Zank, G. P. 2003, ApJL, 590, L53
McKibben, R. B. 1972, JGR, 77, 3957
Reid, G. C. 1964, JGR, 69, 2659
Roelof, E. C. 1969, in Lectures in High Energy Astrophysics, NASA SP-199, ed. H. Ogelmann & J. R. Wayland (Washington, DC: NASA), 111
Roelof, E. C., Gold, R. E., Simnett, G. M., et al. 1992, GeoRL, 19, 1243
Ruffolo, D. 1995, ApJ, 442, 861
Schlickeiser, R. 2002, Cosmic Ray Astrophysics (Berlin: Springer)
Schlickeiser, R., & Shalchi, A. 2008, ApJ, 686, 292
Shalchi, A. 2010, ApJL, 720, L127
Shalchi, A. 2019, ApJL, 881, L27
Shalchi, A., Bieber, J. W., Matthaeus, W. H., & Schlickeiser, R. 2006, ApJ, 642, 230
Shalchi, A., & Danos, R. J. 2013, ApJ, 765, 153
Shalchi, A., & Schlickeiser, R. 2005, ApJL, 626, L97
Shalchi, A., Škoda, T., Tautz, R. C., & Schlickeiser, R. 2009, A&A, 507, 589
Tautz, R. C., Shalchi, A., & Dosch, A. 2014, ApJ, 794, 138
Zhang, M., Qin, G., & Rassoul, H. 2009, ApJ, 692, 109